RZ 2803 (# 90106) 04/08/96
Physical Sciences 8 pages

Research Report

Implications of XY–Critical Point Behavior for the Properties of High-T_c Cuprates

T. Schneider*†, Y. Jaccard‡, J.-P. Locquet*, P. Martinoli‡ and Ø. Fischer§

*IBM Research Division
Zurich Research Laboratory
8803 Rüschlikon
Switzerland

†Physik-Institut
Universität Zürich
8057 Zürich
Switzerland

‡Institut de Physique
Université de Neuchâtel
2000 Neuchâtel
Switzerland

§Dép. de Physique
de la Matière Condensée
Université de Genève
1211 Genève
Switzerland

Research Division
Almaden · T.J. Watson · Tokyo · Zurich

Implications of XY–Critical Point Behavior for the Properties of High-T_c Cuprates

T. Schneider*†, Y. Jaccard‡, J.-P. Locquet*, P. Martinoli‡ and Ø. Fischer§

IBM Research Division, Zurich Research Laboratory, 8803 Rüschlikon, Switzerland

†*Physik-Institut, Universität Zürich, 8057 Zürich, Switzerland*

‡*Institut de Physique, Université de Neuchâtel, 2000 Neuchâtel, Switzerland*

§*Dép. de Physique de la Matière Condensée, Université de Genève, 1211 Genève, Switzerland*

Abstract: The analysis presented here affords a new perspective on the implications of the phase diagram and the nature of the superconducting state in cuprate superconductors. We invoke the mapping of this state onto the anisotropic three-dimensional (3D)–XY model, supplemented by the experimental doping dependence, the effective mass anisotropy parameter and the fact that the cuprates undergo an insulator–to–superconductor and superconductor–to–normal-state transition at zero temperature. On this basis we show that the materials undergo at zero temperature a crossover from Bose–Einstein condensation to BCS-type behavior as the hole concentration increases from the underdoped to the overdoped limit, combined with a dimensional crossover from 2D–XY to anisotropic 3D–XY critical behavior. Moreover, using the critical properties and the phase transition line, we estimate the doping dependence of the penetration depth λ, transverse correlation length, and specific heat singularity, in remarkable agreement with the available experimental data. The resulting relation between transition temperature and λ^{-2} reveals the generic significance of this scenario.

Considerable debate has arisen over the doping dependence of the transition temperature T_c [1,2] and magnetic penetration depth λ [3–5] of cuprate superconductors as well as the resulting correlation between these properties. In these materials, characterized by a complex order parameter, fluctuations are known to be essential. [6–13] Here we explore the mapping of these superconductors onto the anisotropic three-dimensional (3D)–XY model, supplemented by the experimentally established doping dependence of the effective mass anisotropy and the fact that the bulk transition vanishes at the underdoped and overdoped limits.

This paper is organized as follows: First, we present the experimental evidence, revealing that cuprate superconductors and uncharged superfluids like ^{4}He share the universal properties of the XY model in the fluctuation-dominated regime. [14,15] Then we explore the implication of these properties, extended to the anisotropic XY model, [6,7] and supplemented by the experimental facts that the materials undergo a dimensional crossover from 2D to 3D–XY critical behavior and exhibit an insulator–superconductor and superconductor–normal-state transition at zero temperature as the hole concentration increases. The implications include: (i) A universal 2D resistance $h^2/4e^2$ in the underdoped limit as observed experimentally; [16] (ii) Given the doping dependence of the transition temperature T_c, the behavior of the magnetic penetration depth λ, correlation length, and specific heat singularity is related to the crossover from Bose–Einstein condensation (BEC) to BCS superconductivity at zero temperature. This crossover provides a natural explanation of a variety of measurements, including NMR [17] and optical conductivity [18] on underdoped materials, revealing the existence of a pseudogap above the transition temperature. (iii) An explanation of the relation between T_c and λ^{-2} emerging from muon-spin relaxation experiments. [3,4,7,8]

Measurements of various properties, including the specific heat [7,9,10] and the magnetic penetration depth, [5,11] strongly suggest that in the Meissner phase and close to the transition temperature, the fluctuations of the order parameter are essentially those of a neutral superfluid or 3D–XY model. The associated complex order parameter field $\Psi(\vec{r})$ represents the macroscopic wave function of singlet pairs of charge $2e$. Introducing the magnetic penetration depth λ, the correlation length ξ describing the decay of the fluctuations in the modulus $|\Psi(\vec{r})|$, and concentrating on the fluctuation-dominated temperature regime, the uncharged behavior of the cuprates can be understood in terms of the dimensionless charge $\tilde{e} = 1/\kappa = \xi/\lambda$. [7,12] In these materials, this charge is small because $\lambda \gg \xi$. [7] Nevertheless, owing to the pronounced effective mass anisotropy of the cuprates, the isotropic XY model is not directly applicable. Indeed, according to the available magnetic torque measurements, γ adopts rather large values: $\gamma \approx 5$: $YBa_2Cu_3O_{6.97}$, [19] $\gamma \approx 20$: $La_{2-x}Sr_xCuO_4$, [20] and $\gamma > 150$: $Bi_2Sr_2CaCu_2O_8$. [21] The parameter $\gamma = \sqrt{M_\perp/M_\|}$ characterizes the anisotropy of the effective mass perpendicular ($\perp$) and parallel ($\|$) to the layers.

For this reason we perform in the fluctuation-dominated regime the mapping of the superconducting state onto the 3D–XY model with pronounced uniaxial anisotropy. In this case the bulk transition temperature T_c^{3D} falls with increasing γ as the system crosses over from the 3D–XY to the 2D–XY critical point, where at T_{KT} a Kosterlitz–Thouless transition occurs. [22,23]

Next we introduce the experimental ingredients, namely the doping dependence of the anisotropy parameter γ and the fact that T_c vanishes at the underdoped and overdoped limits. There is considerable evidence that the phase transition line of all hole-doped cuprate superconductors, i.e. T_c^{3D} versus the concentration x of holes per unit CuO_2 in the CuO_2 layer, is of the form sketched in Fig. 1. [1,2] The temperature $T_c^{3D}(x)$ attains its maximum value T_c^m at x_m and vanishes at the underdoped (x_u) and overdoped (x_o) limits. At $T = 0$, the materials undergo at x_u an insulator–to–superconductor and at x_o a superconductor–to–normal-state transition. In most materials, however, only part of this line is experimentally accessible. The measured resistivity anisotropy ratio $\rho_\perp/\rho_\parallel \propto \gamma^2$ reveals that cuprate superconductors become more metallic and isotropic in the overdoped regime. [24,25] This behavior is fully consistent with the anisotropic 3D–XY model because T_c^{3D}/T_{KT} increases if γ decreases. [22,23] Indeed, with decreasing anisotropy γ, the system becomes more isotropic and the corresponding rise of T_c^{3D}/T_{KT} reflects the suppression of 2D fluctuations. Thus, at $T = 0$ and $x = x_u$, corresponding to the critical point 1, an insulator–to–metal transition occurs, [16] the materials are 2D and the resistance is universal. [26] For $x > x_u$, however, $\gamma(x)$ decreases and drives the crossover from 2D–XY to 3D–XY up to the critical point 2, where the materials undergo a superconductor–to–normal-state transition (Fig. 1). With the exception of these end points, the materials are expected to exhibit along the phase transition line anisotropic 3D–XY critical behavior.

In the remainder of this work, we analyze the 3D–XY critical line and its end points 1 and 2 by means of the universal critical point relations at finite and zero temperature. The consequences will turn out to be considerable. Indeed, given the doping dependence of T_c, the corresponding behavior of the magnetic penetration depth λ, transverse correlation length and specific heat as well as the relation between T_c and $1/\lambda^2$ simply follow.

Approaching a critical point for fixed x from below T_c (see Fig. 1), the transverse correlation length and the parallel magnetic penetration diverge as $\xi_\parallel^T(T) = \xi_{\parallel 0}^T t^{-\nu}$ and $\lambda_\parallel^2(T) = \lambda_{\parallel 0}^2 t^{-\nu}$, where $t = 1 - T/T_c^{3D}$ and $\nu \approx 2/3$. Moreover, T_c^{3D} and the magnetic bulk penetration depth $\lambda_\parallel$ are not independent properties, but related by [6,7,15]

$$k_B T_c^{3D} = \frac{\Phi_0^2}{16\pi^3} \frac{\xi_{\parallel 0}^T}{\lambda_{\parallel 0}^2} \quad . \tag{1}$$

There is also the relation [6,7]

$$R_T^3 = A^-(\xi_{\parallel 0}^T)^2\, \xi_{\perp 0}^T = (0.8)^3 \quad , \qquad \frac{\xi_{\parallel 0}^T}{\xi_{\perp 0}^T} = \frac{1}{\gamma^2} \quad , \tag{2}$$

which connects the amplitude $A^+ \approx A^-$ of the specific heat singularity $C^\pm = (A^\pm/\alpha)\,|t|^{-\alpha}$ with the volume of the transverse correlation lengths.

To estimate the doping dependence of $\lambda_{\parallel 0}$ and $\xi_{\parallel 0}^T$, we invoke the critical behavior of $T = 0$. With increasing x the cuprates undergo at 1 a 2D insulator–metal transition and at 2 a superconductor–normal-state transition (Fig. 1). In contrast to finite temperatures, for which static critical phenomena can be discussed with no regard to the systems dynamics, the fluctuations at zero temperature are of a purely quantum mechanical nature, so static and dynamic quantities are linked. Near the insulator–to–superconductor transition 1 the cuprates are 2D and the magnetic penetration depth and transverse correlation length are expected to scale as $\lambda_\parallel^2(T=0) = a_{\lambda u}(x - x_u)^{-1}$, $\xi_\parallel^T(T=0) = \xi_{\parallel o}^T(x - x_u)^{-1/2}$, respectively. [26] This transition can be regarded as a boson localization problem, in which the pairs are localized below and delocalized above x_u, and superconductivity arises due to BEC. At finite temperature, close to x_u, and below a mean-field transition temperature, the electrons form pairs, but the true transition temperature is lowered by the enhanced phase fluctuations in two dimensions. A characteristic signature of this transition is the existence of two energy scales, namely the binding energy of the pairs $k_B T^*$ and their condensation energy $k_B T_c^{3D}$, where $T_c^{3D} < T^*$. In the temperature range $T_c^{3D} < T < T^*$ the effects of pairing manifest themselves as a suppression of low-energy excitations, i.e. as a pseudogap. The existence of a pseudogap opening below T^* is well confirmed by a variety of measurements, including NMR [17] and optical conductivity. [18]

Approaching x_o the cuprates become more isotropic and undergo at 2 a superconducting–normal-state transition (Fig. 1). The experimental fact of rather metallic normal–state properties, [24] requires $T_c^{3\mathrm{D}} \approx T^*$, i.e. that electron pairing and long-range phase coherence occur at the same temperature. For this reason we are left with BCS-type behavior, namely $\lambda_{||}^2(T=0) = a_{||\mathrm{o}}(x_\mathrm{o}-x)^{-1}$, $\xi_{||}^T(T=0) = \xi_{||\mathrm{o}}^T(x_\mathrm{o}-x)^{-1/2}$.
From finite size scaling at the critical points 1 and 2 in the time direction and Eq. (1) it follows that the zero and finite temperature critical amplitudes exhibit the same doping dependence. To cover the full doping regime, we interpolate between the critical points in terms of the ansatz

$$\lambda_{||0}^2(x) \approx \frac{a_{\lambda\mathrm{u}}^2}{x-x_\mathrm{u}} + \frac{a_{\lambda\mathrm{o}}^2}{x_\mathrm{o}-x} \quad , \qquad \xi_{||0}^T(x) \approx \left(\frac{\xi_{||\mathrm{u}}^T}{\sqrt{x-x_\mathrm{u}}} + \frac{\xi_{||\mathrm{o}}^T}{\sqrt{x_\mathrm{o}-x}} \right) \quad . \tag{3}$$

which will be justified *a posterior*.
Now for any finite temperature and $x > x_\mathrm{u}$, the universal relations (1) and (2) apply. Accordingly the doping dependence of the critical properties, reflecting the crossover phenomena, are fully controlled by the amplitudes $a_{\lambda\mathrm{u}}$, $a_{\lambda\mathrm{o}}$, $\xi_{||\mathrm{u}}^T$, $\xi_{||\mathrm{o}}^T$, and the anisotropy parameter $\gamma(x)$. To estimate the magnitude of these amplitudes we use the rather extended experimental data for the doping dependence of $T_c^{3\mathrm{D}}$ in bulk $La_{2-x}Sr_xCuO_4$. [27–29] The data and the fit to Eqs. (1) and (3) are shown in Fig. 2, yielding the estimates for the ratios $\xi_{||\mathrm{u}}^T/a_{\lambda\mathrm{o}}$, $\xi_{||\mathrm{o}}^T/\xi_{||\mathrm{u}}^T$, and $a_{\lambda\mathrm{o}}/a_{\lambda\mathrm{u}}$. For comparison we included the data of high-quality films, 390 to 520 Å thick. [5] The reduced doping range and the lower transition temperature of the films has been attributed to substrate-induced stress. [30] The slight asymmetry of $T_c^{3\mathrm{D}}(x)$ reflects the small value of the amplitude ratio $\xi_{||\mathrm{o}}^T/\xi_{||\mathrm{u}}^T \approx 0.085$. As shown in Fig. 3, this small ratio leads to a manifestly asymmetric doping dependence of $\xi_{||0}^T$. To obtain $\xi_{||0}^T(x)$ from Eq. (3) and the fitted amplitude ratios we used the experimental value $\lambda_{||0}(x=0.15) \approx 2250$ A, [7,31] yielding $a_{\lambda\mathrm{u}} = 3.06 \times 10^5$ A^2, $a_{\lambda\mathrm{o}} = 2.2 \times 10^5$ A^2, $\xi_{||\mathrm{u}}^T \approx 0.83$ A and $\xi_{||\mathrm{o}}^T \approx 0.07$ A. "Experimental" estimates for $\xi_{||0}^T$ have been derived from a finite size scaling analysis of $\lambda_{||}(T)$ in thin films. [5] The inset in Fig. 3 shows that the film data reveals a less pronounced asymmetry. More importantly, the raise of $\xi_{||0}^T(x)$ in the underdoped and overdoped limits is well confirmed and strongly affects the critical amplitude of the specific heat singularity, given by $A^-(x) \propto \gamma(x)^{-2}(\xi_{||0}^T(x))^3$, (Eq. (2)). Experimental evidence for the resulting reduction of A^- comes from specific heat measurements of underdoped $YBa_2Cu_3O_{7-x}$. [32]
The doping dependence of $\lambda_{||0}$ is depicted in Fig. 4 and, for comparison, we included the μSR bulk estimates. [7,31] The inset shows the kinetic induction measurements of high-quality films. [5,6] In contrast to the transverse correlation length amplitude, the asymmetry in the doping dependence is much less pronounced, because $a_{\lambda\mathrm{o}}/a_{\lambda\mathrm{u}} \approx 0.717$. This feature is well confirmed by the film data. The divergence of $\lambda_{||0}$ in both the underdoped ($x \to x_\mathrm{u}$) and overdoped ($x \to x_\mathrm{o}$) limits follows from the zero-temperature phase diagram (Eq. (3)). In the overdoped limit it invalidates the standard assumption: that proportionality exists between hole concentration $x - x_\mathrm{u}$ and superfluid density n_s. Indeed, $1/\lambda_{||0}^2 \propto n_\mathrm{s}/M_{||}$ and $n_\mathrm{s} \propto x - x_\mathrm{u}$ imply with Eq. (3) that $M_{||} \to \infty$ for $x \to x_\mathrm{o}$. However, such a heavy effective mass contradicts the experimental fact that cuprate superconductors become more metallic in the overdoped regime. [24]
To provide evidence of the generic significance of these crossover phenomena we consider the plot $\overline{T}_c^{3\mathrm{D}} = T_c^{3\mathrm{D}}/T_c^\mathrm{m}$ versus $(\lambda_{||0}^m/\lambda_{||0})^2 = \overline{\lambda}_{||0}^{-2}$. The solid and dashed curves, which resemble the outline of a fly's wing, have been obtained with the aid of Eqs. (1) and (3) and the aforementioned parameters for bulk $La_{2-x}Sr_xCuO_4$. The arrows denote the evolution of a system as x increases from the underdoped ($\uparrow$, $x_\mathrm{u} \leq x \leq x_\mathrm{m}$) to the overdoped ($\downarrow$, $x_\mathrm{m} \leq x \leq x_\mathrm{o}$)

regimes. The width of the wing reflects the asymmetry in the doping dependence of $\lambda_{\|0}$ and $T_c^{3D}(x)$ (see Figs. 2 and 4). To demonstrate the generic significance of this behavior we included the available μSR data of various cuprates in terms of $\sigma_{\|}(T=0) \propto 1/\lambda_{\|}^2(T=0)$, where $\lambda_{\|}^2(T=0)$ is taken as a measure for $\lambda_{\|0}^2$. The parameter σ is the μSR relaxation rate. Indeed, the experimental points of overdoped $La_{2-x}Sr_xCuO_4$ [8] and $Tl_2Ba_2CuO_{6+\delta}$ [3,4] confirm the essential feature namely, reversed evolution of underdoped (up) and overdoped (down) systems, which resembles the outline of a fly's wing.

The analysis presented here affords a new perspective on the doping dependence of various properties and the nature of the superconducting state in cuprate superconductors. We invoked the mapping onto the anisotropic 3D–XY model, supplemented by the experimental doping dependence, the effective mass anisotropy parameter γ, and the fact that cuprates undergo an insulator–to–superconductor and superconductor–to–normal-state transition at zero temperature. On this basis we have shown that the ground state undergoes a crossover from BEC to BCS-type behavior as the hole concentration increases from the underdoped to the overdoped limit, combined with a dimensional crossover from 2D–XY to anisotropic 3D–XY critical behavior. Given the phase transition line T_c^{3D} of $La_{2-x}Sr_xCuO_4$, we estimated the doping dependence of the penetration depth, transverse correlation length, and specific heat singularity, in remarkable agreement with available experimental data. The resulting relation between T_c^{3D} and $\lambda_{\|0}^{-2}$ revealed the generic significance of this scenario.

We thank many colleagues for insightful suggestions, questions, and comments. Those who contributed include H. Beck, A. Junod, M. Büttiker, H. Keller, R. Micnas, K. A. Müller, M. H. Pedersen, Ch. Rossel, J. Singer, J. M. Triscone, and D. Zech.

---

[1] Tallon, J. L. & Flower, N. E. *Physica C* **204**, 237-246 (1993).

[2] Zhang, H. & Sato, H. *Phys. Rev. Lett.* **70**, 1697-1699 (1993).

[3] Niedermeier, Ch., Bernhard, C., Binninger, U., Glückler, H., Tallon, J. L., Ansaldo, E. J. & Budnick, J. I. *Phys. Rev. Lett.* **7**, 1764-1767 (1993).

[4] Uemura, Y. J., Keren, A., Lee, L. P., Luke, G. M., Wu, W. D., Kubo, Y., Manako, T., Shimakawa, Y., Subramanian, M., Cobb, J. L. & Markert, J. T. *Nature* **364**, 605-607 (1993).

[5] Jaccard, Y., Schneider, T., Locquet, J.-P., Williams, E. J., Martinoli, P. & Fischer, Ø. preprint.

[6] Schneider, T. & Ariosa, D. *Z. Phys. B* **89**, 267-274 (1992).

[7] Schneider, T. & Keller, H. *Int'l J. Mod. Phys. B* **8**, 487-528 (1994).

[8] Bednorz, G. & Keller, H. private communication.

[9] Kozlowski, A., Tarnawski, Z., Kolodziejczyk, A., Chmist, J., Scizor, T. & Zalecki, R. *Physica C* **184**, 113-118 (1991).

[10] Overend, N., Howsen, M. A. & Lawrie, I. D. *Phys. Rev. Lett.* **72**, 3238-3241 (1994).

[11] Kamal, S., Bonn, D. A., Goldenfeld, N., Hirschfeld, P. J., Liang, R. & Hardy, N. W. *Phys. Rev. Lett.* **73**, 1843-1848 (1994).

[12] Fisher, D. S., Fisher, M. P. A. & Huse, D. A. *Phys. Rev. B* **43**, 130-159 (1991).

[13] Emery, V. J. & Kivelson, S. A. *Nature* **374**, 434-437 (1995).

[14] Fisher, M. E. *Rev. Mod. Phys.* **46**, 597-616 (1974).

[15] Hohenberg, P. C., Aharony, A., Halperin, B. I. & Siggia, E. D. *Phys. Rev. B* **13**, 2986-2996 (1976).

[16] Fukuzumi, Y., Mizuhashi, K., Takenaka, K. & Uchida, S. *Phys. Rev. Lett.* **76**, 684-687 (1996).

[17] Mehring, M. *Appl. Mag. Reson.* **3**, 383-421 (1992).

[18] Wachter, P., Bucher, B. & Pittini, R. *Phys. Rev. B* **49**, 13164-13171 (1994).

[19] Janossy, B., Prost, D., Pekker, S. & Fruchter, L. *Physica C* **181**, 51-56 (1991).

[20] Chien, T. R., Datars, W. R., Veal, B. W., Paulikas, A. P., Kostic, P., Gu, Chun & Jiang, Y. *Physica C* **229**, 273-279 (1994).

[21] Huang, Z. J., Xue, Y. Y., Meng, R. L. & Chu, C. W. *Phys. Rev. B* **49**, 4218-4221 (1994).

[22] Chui, S. T. & Giri, M. R. *Phys. Lett. A* **128**, 49-51 (1988).

[23] Tanner, A., Doctoral Thesis, University of Zurich (1994).

[24] Iye, Y. in *Physical Properties of High Temperature Superconductors III*, edited by Ginsberg, D. M. (World Scientific, Singapore, 1992) 285-361.

[25] Kimura, T., Kishio, K., Kobayashi, T., Nakayama, Y., Motohira, N., Kitazawa, K. & Yamafuji, K. *Physica C* **192**, 247-252 (1992).

[26] Fisher, M. P. A., Weichman, P. B., Grinstein, G. & Fisher, D. S. *Phys. Rev. B* **40**, 546-570 (1989).

[27] Torrance, J. B., Bezinger, A., Nazzal, A. I., Huang, T. C., Parkin, S. S. P., Keane, D. T., LaPlaca, S. J., Horn, P. M. & Held, G. A. *Phys. Rev. B* **40**, 8872-8877 (1989).

[28] Takagi, H., Ido, I., Ishibashi, S., Uota, M., Uchida, S., & Tochura, Y. *Phys. Rev. B* **40**, 2254-2261 (1989).

[29] Nagano, T., Tomioka, Y., Nakayama, Y., Kishio, K. & Kitazawa, K. *Phys. Rev. B* **48**, 9689-9696 (1993).

[30] Williams, E. J., Cretton, A., Jaccard, Y., Locquet, J.-P., Mächler, E., Martinoli, P. & Ø. Fischer, in *Proc. Microscopy and Microanalysis 1995*, edited by Bailey, G. W., Ellisman, M. H., Hennigar, R. A. & Zaluzec, N. J. (Jones and Begell Publishing, NY, 1995) 382-383.

[31] Uemura, Y. J., Emery, V. J., Moodenbaugh, A. R., Suenaga, M., Johnston, D. C., Jacobsen, A. J., Levandowski, J. T., Brewer, J. H., Kiefel, R. F., Kreitzman, S. R., Luke, G. M., Riseman, T., Stronach, C. E., Kossler, W. J., Kempton, J. R., Yu, X. H., Opie, D. & Schone, H. E. *Phys. Rev. B* **38**, 909-912 (1989).

[32] Ghiron, K., Salamon, M. B., Hubbard, M. A. & Veal, B. W. *Phys. Rev. B* **48**, 16191-16199 (1993).

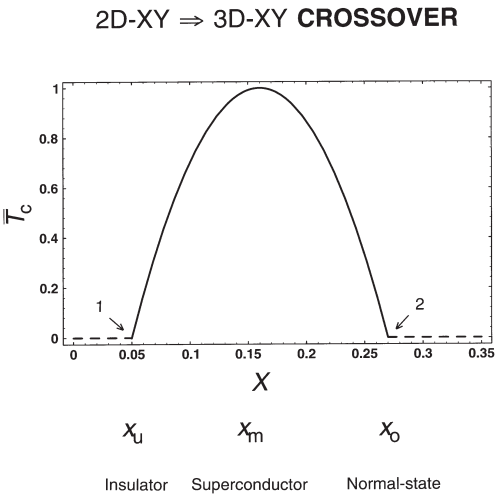

FIG. 1. Schematic phase diagram of cuprate superconductors. At $T = 0$ and with increasing hole concentration x, the materials undergo a 2D to 3D crossover, at x_{u} an insulator–superconductor and at x_{o} a superconductor–to–normal-state transition. 1 denotes the 2D quantum XY critical point of the insulator–to–superconductor transition and 2 the anisotropic 3D quantum XY critical point of the superconductor–to–normal-state transition. 1 and 2 are the end points of the 3D–XY phase transition line.

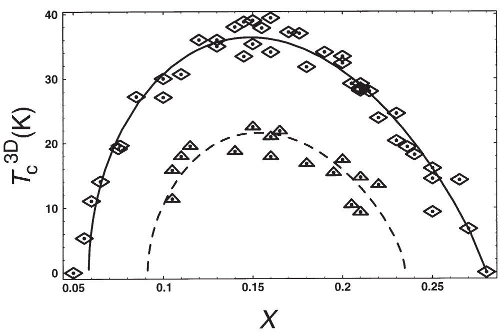

FIG. 2. $T_{\mathrm{c}}^{\mathrm{3D}}$ versus x for $\mathrm{La}_{2-x}\mathrm{Sr}_x\mathrm{CuO}_4$. $\diamond$: bulk data taken from Refs. [27–29]. $\triangle$: Film data taken from Ref. [5]. Solid line: fit from from Eqs. (1) and (3) for $x_{\mathrm{u}} = 0.059$, $x_{\mathrm{o}} = 0.28$, yielding $\xi_{\|\mathrm{u}}^{T}/a_{\lambda\mathrm{o}} \approx 2.7 \times 10^{-6}$ A^{-1}, $\xi_{\|\mathrm{o}}^{T}/\xi_{\|\mathrm{u}}^{T} \approx 0.085$ and $a_{\lambda\mathrm{o}}/a_{\lambda\mathrm{u}} \approx 0.717$; the maximum $T_{\mathrm{c}}^{\mathrm{m}} \approx 36.34$ K occurs at $x \approx 0.15$. Dashed line: from Eqs. (1) and (3) for $x_{\mathrm{u}} \approx 0.09$, $x_{\mathrm{o}} \approx 0.235$, $\xi_{\|\mathrm{u}}^{T} \approx 2.92$ A, $\xi_{\|\mathrm{o}}^{T} \approx 1.51$ A, $a_{\lambda\mathrm{o}} \approx 1.703 \times 10^{6}$ A^{2} and $a_{\lambda\mathrm{u}} \approx 1.772 \times 10^{6}$ A^{2}. The estimates for the amplitudes of the films have been derived from Eq. (3) and the experimental data for $\lambda_{\|0}(x)$ and $\xi_{\|0}^{T}(x)$. [5]

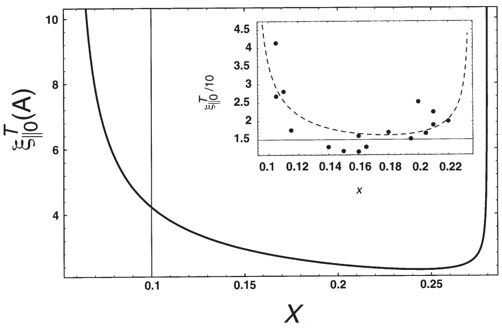

FIG. 3. $\xi^T_{||0}$ versus x for $La_{2-x}Sr_xCuO_4$ derived from Eqs. (1) and (3) for $\xi^T_{||u} \approx 0.83$ A and $\xi^T_{||o} \approx 0.07$ A. The minimum $\xi^T_{||0} \approx 2.3$ A occurs at $x = 0.244$. The inset shows the experimental data of $La_{2-x}Sr_xCuO_4$ films. [5] The dashed line is a fit to Eq. (5) for $x_u \approx 0.095$, $x_o \approx 0.235$, yielding $\xi^T_{||u} \approx 2.92$ A and $\xi^T_{||o} \approx 1.51$ A. The minimum $\xi^T_{||0} \approx 17$ A occurs at $x = 0.18$.

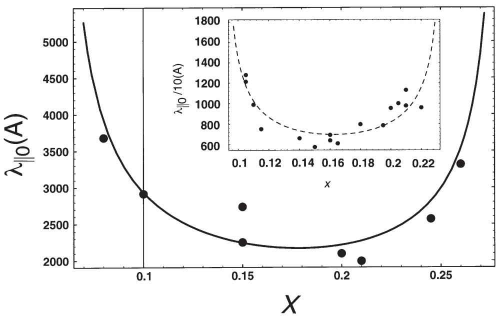

FIG. 4. $\lambda_{||0}$ versus x for $La_{2-x}Sr_xCuO_4$. •: measured bulk data taken from Refs. [8] and [31]; Solid line: derived from Eqs. (1) and (3) for $a_{\lambda u} \approx 3.06 \times 10^5$ A^2 and $a_{\lambda o} \approx 2.2 \times 10^5$ A^2. The minimum $\lambda_{||0} \approx 2172$ A occurs at $x = 0.178$. The inset shows the film data [5] with a fit to Eq. (3) for $x_u \approx 0.09$, $x_o \approx 0.235$, yielding $a_{\lambda o} \approx 1.77 \times 10^6$ A^2 and $a_{\lambda u} \approx 1.7 \times 10^6$ A^2 (dashed line). The minimum $\lambda_{||0} \approx 6959$ A occurs at $x \approx 0.16$.

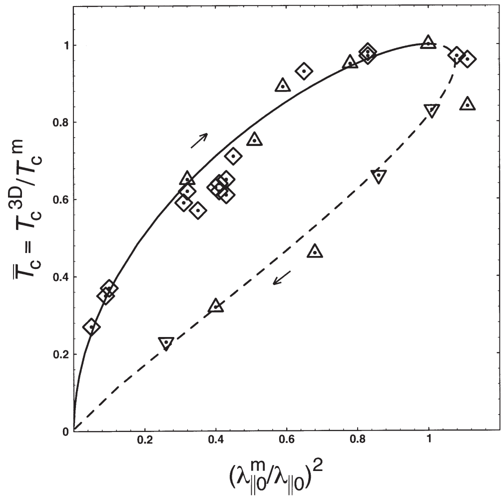

FIG. 5. $\overline{T}_c^{3D}$ versus $(\lambda_{\|0}^{m}/\lambda_{\|0})^2$. Solid line: underdoped branch and dashed line: overdoped branch according to Eqs. (1) and (3) for bulk $La_{2-x}Sr_xCuO_4$ for the critical amplitudes used in Figs. 2 and 4. The arrows indicate the crossover from the underdoped (up) to the overdoped (down) limit. The other symbols are μSR data in terms of $\overline{T}_c$ versus $\overline{\sigma}(T=0) = (\lambda_{\|}^{m}(T=0))^2/\lambda_{\|}(T=0)$, taken from Refs. [3,4,7,8,31].

$\bigtriangledown$: $La_{2-x}Sr_xCuO_4$.

$\bigtriangleup$: $Tl_2Ba_2CuO_{6+\delta}$.

$\diamond$: $YBa_2Cu_3O_{7-\delta}$.